

Structure of odd- A Pt isotopes along the line of stability

S.G. Wahid,¹ S.K. Tandel^{a,1,2} P. Chowdhury,² R.V.F. Janssens,^{3,4}

M.P. Carpenter,⁵ T.L. Khoo,⁵ F.G. Kondev,⁵ T. Lauritsen,⁵ C.J.

Lister,^{2,5} D. Seweryniak,⁵ S. Zhu,⁵ Q.B. Chen,⁶ and J. Meng⁶

¹*School of Physical Sciences, UM-DAE Centre for Excellence in Basic Sciences,
University of Mumbai, Mumbai 400098, India*

²*Department of Physics, University of Massachusetts
Lowell, Lowell, Massachusetts 01854, USA*

³*Department of Physics and Astronomy,
University of North Carolina at Chapel Hill,
Chapel Hill, North Carolina 27599, USA*

⁴*Triangle Universities Nuclear Laboratory,
Duke University, Durham, North Carolina 27708, USA*

⁵*Argonne National Laboratory, Argonne, Illinois 60439, USA*

⁶*State Key Laboratory of Nuclear Physics and Technology,
School of Physics, Peking University, Beijing 100871, China*

(Dated: December 28, 2018)

Abstract

The structure of the odd- A isotopes $^{193,195,197}\text{Pt}$, which lie along the line of stability, has been studied up to high spin through multi-nucleon transfer reactions. Positive- and negative-parity sequences in $^{193,195}\text{Pt}$ have been considerably extended and multiple band crossings established. An isomer with $T_{1/2} = 5.0(5)$ ns and $I^\pi = 25/2^-$ is present in ^{195}Pt . The isotopes $^{193,195}\text{Pt}$ are characterized by moderate oblate deformation, and angular momentum generation at high spin in the yrast, positive-parity sequences is attributed to the rotation alignment of $i_{13/2}$ neutrons and $h_{11/2}$ protons. A detailed understanding of the observed features is presented using calculations based on tilted axis cranking covariant density functional theory as well as others with the Ultimate Cranker code.

PACS numbers: 21.10.Re, 21.60.Ev, 23.20.Lv, 27.80.+w

^a Corresponding author: sujit.tandel@cbs.ac.in , sktandel@gmail.com

I. INTRODUCTION

The structure of nuclei in the $A \approx 190$ -200 region exhibits a complex interplay between collective effects and those due to individual nucleons. These nuclei show evidence of moderate deformation and excited states appear to result from collective rotation [1–3]. However, owing to the small number of valence nucleons, collectivity is not as well developed as, for example, in the deformed, mid-shell $A \approx 170$ -180 region. While most of the Nilsson orbitals are characterized by low- j values due to the presence of high- j , neutron $i_{13/2}$ and proton $h_{11/2}$ subshells in the vicinity of the respective Fermi levels, Coriolis anti-pairing effects lead to rotation-aligned bands, which are the preferred excitation mode at high spin. Additionally, shape coexistence is evident in this region, with a transition from a prolate to an oblate shape with increasing atomic number Z , neutron number N , and spin. Collectivity diminishes when approaching the doubly-magic, spherical nucleus ^{208}Pb . Hence, the $A = 190$ -200 region is of particular interest due to this wide variety of competing effects.

Our previous studies in this region have focused on the even- A isotopes $^{192-198}\text{Pt}$ [2, 3]. Excited states up to $I^\pi = 26^+$ were established and the band structures built on isomeric, 12^+ levels were inferred to have underlying oblate deformation. $B(E2)$ transition probabilities, determined from lifetime measurements, were used to conclude that, while the extent of collectivity decreases gradually near the ground state from $N = 114$ -120, an abrupt drop occurs in the vicinity of the rotation-aligned, 12^+ level near $N = 120$. This is due to intrinsic excitations becoming favored, particularly at high spin, in comparison to collective modes, approaching the neutron shell closure at $N = 126$.

It is of interest to explore the structure of odd- A Pt isotopes for the following reasons. The yrast levels in these isotopes are built on the metastable, $13/2^+$ state resulting from the occupation of the $i_{13/2}$ orbital by the unpaired neutron. Consequently, the first band crossing, with AB neutron character observed in the even- A isotopes, is expected to be blocked due to the Pauli principle. This offers the opportunity to explore the role of other band crossings in generating angular momentum. Further, the effect of the unpaired nucleon on deformation can be explored. The loss of collectivity as the Fermi level approaches $N=120$ determined in the investigation of even- A isotopes [2] can be examined further through a study of the odd- A isotopes $^{193,195,197}\text{Pt}$ with neutron numbers $N=115,117,119$, respectively.

II. EXPERIMENT AND RESULTS

While it is possible to study proton-rich, odd- A Pt isotopes through heavy-ion fusion evaporation [4, 5], those with $A > 192$ can only be accessed using α beams [6–8]. For $A \geq 195$, incomplete fusion, inelastic excitation or multi-nucleon transfer reactions are available mechanisms using stable beams. In the present work, levels at high spin in $^{193,195,197}\text{Pt}$ were populated through multi-nucleon transfer reactions followed by neutron evaporation with a thick ($\approx 50 \text{ mg/cm}^2$) ^{197}Au target and a 1450-MeV ^{209}Bi beam provided by the ATLAS accelerator at Argonne National Laboratory. The Gammasphere detector array [9, 10], comprising 100 high-purity, Compton-suppressed germanium detectors, was used to record three- and higher-fold γ -ray coincidence events. Various multi-dimensional energy and time histograms were created and analyzed to establish the level structure and lifetimes of isomeric states, in addition to the multipolarities of observed transitions. Details about the data analysis may be found elsewhere [2, 3].

Excited states in ^{193}Pt up to the $(37/2^+)$ level were previously established using the $^{192}\text{Os}(\alpha,3n\gamma)$ reaction [7]. The negative-parity sequence was identified up to the $29/2^{(-)}$ level. Additionally, several non-yrast states were also established. The isotope ^{195}Pt was studied following incomplete fusion of ^7Li on a ^{192}Os target and levels up to $(25/2^+)$ in the positive-parity band built on the $13/2^+$ isomeric state, and up to $33/2^-$ in the negative-parity sequence, were determined [8]. In the case of ^{197}Pt , a few levels populated following the decay of an isomer were identified in the fragmentation of a 1 GeV/nucleon ^{208}Pb beam [11].

A. ^{193}Pt

The decay scheme of ^{193}Pt has been extended up to an excitation energy of 4.8 MeV with the inclusion of thirteen previously unobserved γ rays (Fig. 1). The positive-parity sequence is observed to fork into multiple branches, with states up to a tentative spin of $(53/2^+)$ identified. Transitions above the $37/2^+$ level are illustrated in the coincidence spectra of Fig. 2 with simultaneous gates on: (a) the known 341- and 703-keV γ rays, where all newly observed transitions are visible, and (b) the newly identified 448-keV γ ray along with a few transitions at lower spin in the positive-parity band, to highlight one of the

observed branches. Relative intensities of transitions assigned to ^{193}Pt are listed in Table I. From the previous work [7], the spin-parity of the level at 2696 keV had been assigned as $33/2^+$. This is confirmed in the present work. Based on DCO (Directional Correlation of Oriented States) ratios obtained in this work, a quadrupole character is inferred for the 433- and 344-keV γ rays in the yrast, positive-parity sequence. The levels at 3129 and 3473 keV in this sequence are, therefore, assigned spin-parity $37/2^+$ and $41/2^+$, respectively. Beyond the $41/2^+$ state at 3473 keV, insufficient information on DCO ratios prevents unambiguous assignment of spin. A quadrupole character is tentatively assumed for all γ rays above this level up to the 613-keV transition. The transitions above the 3129-keV level were placed based on observed coincidence relations and ordered according to their estimated total intensities using theoretical values of conversion coefficients [12]. A branching is observed above the $37/2^+$ level with a cascade of transitions having energies 466, 221, 718 and 198 keV in addition to a 672-keV γ ray. Spin-parity assignments for the associated levels were not possible. The 122-keV transition connecting the 3595- and 3473-keV levels was not observed most likely since the transition is weak and highly converted. Its placement in the level scheme is validated by the observed coincidences between the transitions below and above the 3473- and 3595-keV levels. The 198-keV transition, though it has a higher γ -ray intensity, is placed above the 718-keV γ ray based on the observed coincidences between this and the 448- and 279-keV transitions; the connecting transition/s are below the sensitivity limit of this experiment. The 672- and 718-keV γ rays, unlike the 198-keV one, are not observed to be coincident with the 279- and 448-keV transitions. Two other γ rays with energies 218 and 479 keV were also observed in the coincidence spectra but could not be placed in the level scheme.

The previously observed levels in the negative-parity sequence, including the isomeric, $25/2^{(-)}$ state at 1455 keV, are confirmed in the present work. The half-life of this state is determined to be 3.3(4) ns, which is the weighted mean obtained from the difference in time of three pairs of transitions below and above this level, using the centroid shift method (Fig. 3). This is consistent with the previously reported value of 3.1(5) ns [7]. The negative-parity sequence is extended from spin-parity $29/2^{(-)}$ to $(39/2^-)$ with the observation of several new γ rays which are illustrated in Figs. 1 and 2. The newly established sequence built on the $27/2^{(-)}$ state at 1690 keV is most likely a signature-partner band of the one built on the $25/2^{(-)}$ level at 1455 keV, based on the similarity of the energy spacings and

the observed connecting, $\Delta I=1$ transitions. It is also quite similar to the negative-parity, signature-partner sequences observed in ^{191}Pt [5].

B. ^{195}Pt

Levels up to an excitation energy of 5.7 MeV have been established in ^{195}Pt with the addition of fifteen previously [8] unobserved transitions (Fig. 4). The sequence built on the isomeric, $13/2^+$ state has been extended with the inclusion of the 773-keV, $(29/2^+) \rightarrow (25/2^+)$ γ ray. No transitions were observed to feed the $(29/2^+)$ state. This is not unexpected as will be discussed below. The level at 2957 keV deexcites to the negative-parity sequence via the 365-keV γ ray (Fig. 5) for which a dipole character is inferred from its DCO ratio (Table I). A rotational-like sequence of six transitions, built on the state at 2957 keV, has been established (Fig. 5). Electric dipole character for the 365-keV γ ray and therefore positive parity is suggested for all levels in this sequence based on the systematic behavior observed in neighboring odd- A isotopes. A more detailed discussion about this aspect is presented later. The 226-keV transition deexciting the 3183-keV level is determined to have quadrupole character (Table I), implying a most likely $37/2^+$ spin-parity assignment for this level. DCO ratios could not be obtained for the higher-lying transitions and an $E2$ character is assumed for all γ rays in this sequence, in analogy with observations in nuclei in this region. The positive-parity sequence is extended up to the $(57/2^+)$ level at 5709 keV.

The $25/2^-$ state at 1536 keV had been identified in previous work [8]. However, its half-life had not been reported. Since the $25/2^-$ level is isomeric in $^{191,193,197}\text{Pt}$, histograms of the time difference between γ rays above and below this state were inspected. These were found to present distinct evidence for a shift in the centroid when compared to prompt transitions of similar energy (Fig. 3). The magnitude of the centroid shift implies a half-life $T_{1/2} = 5.0(5)$ ns. Several transitions are observed to feed the $33/2^-$ level at 2592 keV. While γ -ray coincidence relationships clearly establish the placement of various transitions, owing to the absence of DCO ratios, spin-parity assignments were not possible. The 174-, 860-, 662- and 381-keV transitions are ordered according to their total intensities.

C. ^{197}Pt

Three transitions above the $13/2^+$ level had been previously observed from the decay of an isomeric state in ^{197}Pt populated through projectile fragmentation [11]. The half-life of this isomeric level had been reported to be 10.2(13) ns. This value is consistent with the one from the present measurement ($T_{1/2} = 9.4(5)$ ns). Fig. 6 displays the time distribution of cumulative intensity of γ rays deexciting this isomer. A spin-parity ($25/2^-$) is suggested for this state. This is similar to observations in the lighter, odd- A Pt isotopes. The energy separation between the ($25/2^-$) and ($21/2^-$) levels is most likely small (< 100 keV), herewith precluding observation of the associated transition. Four new γ rays were established to feed the isomeric state (Fig. 6). The spins for the corresponding levels could not be assigned.

III. DISCUSSION

A. Isomers in the Pt isotopes

Isomers, with half-lives in the 1-10 ns range, have been established in both even- and odd- A Pt isotopes. These are in addition to the long-lived, $13/2^+$ spin isomers in odd- A Pt isotopes, arising from the occupation of the $i_{13/2}$ orbital by the unpaired neutron. In even- A isotopes, $I^\pi=7^-$ states are known to have isomeric character, with $T_{1/2} = 1.85(17)$, $3.45(12)$, $5.2(2)$ and $3.4(2)$ ns in $^{192,194,196,198}\text{Pt}$, respectively [2, 3, 13–17]. This situation is mirrored in the odd- A Pt isotopes, where the $I^\pi = 25/2^-$ levels are isomers with $T_{1/2} = 1.07(6)$, $3.3(4)$, $5.0(5)$ and $9.4(5)$ ns in $^{191,193,195,197}\text{Pt}$, respectively [7, 11, 16]. The half-life of the $25/2^-$ level in ^{195}Pt measured in the present work fits quite well into the overall systematic trend. In the above Pt isotopes (particularly the heavier ones), these negative-parity states result from a semi-decoupled $\nu^2(i_{13/2}, f_{5/2}$ or $p_{3/2})$ 2-quasiparticle (qp) configuration coupled to a 0-qp and 1-qp $\nu i_{13/2}$ one in the even- and odd- A isotopes, respectively. In the lighter isotopes, the 2-qp configuration $\pi^2(h_{11/2}, d_{3/2}$ or $s_{1/2})$ is also involved [2]. The isomeric character may be attributed primarily to the low energy of the $25/2^- \rightarrow 21/2^-$ $E2$ transition.

The 12^+ states in the even- A isotopes also exhibit an isomeric character with $T_{1/2} = 2.6(3)$, $6.6(6)$, $7.7(7)$ and $36(4)$ ns in $^{192,194,196,198}\text{Pt}$, respectively [2]. These states result from the full alignment of the intrinsic angular momentum of two $i_{13/2}$ neutrons due to rotation-induced Coriolis anti-pairing effects, particularly in the proton-rich isotopes. Unlike the

negative-parity isomers observed in both even- and odd- A isotopes, there is no evidence for isomeric levels in the positive-parity sequences in the latter case. This may be understood in terms of the considerably larger γ -ray energy of the $E2$ transition in the region of the band crossing in ^{193}Pt that results in a larger transition probability corresponding to expected sub-nanosecond lifetimes. In ^{195}Pt , the rotation-aligned $33/2^+$ state deexcites to the negative-parity band through a transition of $E1$ character, leading to a higher transition rate. A possible explanation of the above observations is presented below in the context of cranking calculations.

B. Yrast, positive-parity levels in the Pt isotopes

A comparison of yrast, positive-parity levels in even- and odd- A isotopes is provided in Fig. 7. It may be noted that in the figure the energy of the $13/2^+$ levels in odd- A isotopes is offset by an amount equal to their respective excitation energies (around a few hundred keV). This allows for a direct comparison of the rotational band structures built on the 0^+ ground state in even- A isotopes and on the yrast, $13/2^+$ isomeric levels in odd- A nuclei. The similarity between the odd- and even-mass isotopes is noteworthy (Fig. 7). The gradual decrease in collectivity, evidenced by an increase in the excitation energy of the 2^+ states in even- A isotopes, is mirrored by the rise in the energy spacing between the $17/2^+$ and $13/2^+$ levels. The reduced collectivity is accompanied by a decrease in the moment of inertia as a result of which the 8^+ and analogous $29/2^+$ levels in even- and odd- A isotopes exhibit a gradual increase in excitation energy. The $33/2^+$ states in the odd- A isotopes are to be compared to the 10^+ levels in even- A nuclei. The decrease in energy of these states up to $N=115, 116$ may be understood in terms of the decrease in the frequency of rotation alignment, as the Fermi level moves towards orbitals with successively lower values of Ω (where Ω is the projection of intrinsic angular momentum along the symmetry axis). Consequently, the rotation-aligned states are favored in energy. As the Fermi level approaches the top of the $i_{13/2}$ subshell, the energy required to realize a rotation-aligned state with a broken pair of $i_{13/2}$ neutrons exhibits an increase. This is reflected in the higher excitation energies of the 10^+ and $33/2^+$ levels at and beyond $N = 117$.

C. Shapes and band crossings

Cranking calculations have been performed using the Ultimate Cranker (UC) code [18] with the Modified Oscillator potential to understand shape evolution and band crossings. Details about the prescription may be found in Ref. [3, 18–21]. A Total Energy Surface plot for ^{193}Pt in the vicinity of the one-quasineutron, $13/2^+$ bandhead state indicates that a moderately deformed oblate shape ($\epsilon_2 = 0.145$, $\gamma = -50^\circ$) is favored (Fig. 8), where ϵ_2 and γ represent the quadrupole deformation and triaxiality parameter, respectively. This energy minimum is found to persist to high spin (Fig. 8), with the value of the triaxiality parameter (γ) eventually moving towards -75° . A similar behavior is evident in ^{195}Pt and is suggestive of a transition from oblate to triaxial rotation at high spin.

Neutron and proton quasiparticle energies have been calculated as a function of rotational frequency. Fig. 9 illustrates these calculations for the case of ^{193}Pt . The first (AB) band crossing visible for $i_{13/2}$ neutrons just above $\hbar\omega = 0.2$ MeV is Pauli blocked in the case of the band built on the $13/2^+$ level in odd- A isotopes. The BC crossing is predicted at slightly higher frequency ($\hbar\omega \approx 0.25$ MeV) and expected to be the first one observed experimentally. The aligned angular momentum due to this BC crossing is expected to be $\approx 10 \hbar$, quite close to the experimental value (Fig. 10), and less than that due to the AB crossing ($\approx 12 \hbar$). The interaction strength at the BC crossing is significantly higher than that at the AB one. As a result, the discontinuity in level energies is less pronounced in odd- A isotopes when compared to even- A ones. Therefore, the $E2$ transition energies near the band crossing in odd-mass isotopes are considerably higher than is the case in even- A nuclei leading to the absence of isomers in the former case, as discussed above. The first band crossing in the case of protons in the $h_{11/2}$ orbital occurs around $\hbar\omega = 0.3$ MeV, and is, therefore, expected to be responsible for the second observed rotation alignment (Fig. 10). Similar behavior is apparent in the Hg isotones in terms of the first crossing frequency and alignment gain (Fig. 10). The second crossing evident in the Pt isotopes (Fig. 10) is not observed in the Hg isotones. This may be attributable to the increase in the proton Fermi energy from Pt ($Z=78$) to Hg ($Z=80$) and the consequent higher value of the $h_{11/2}$ crossing frequency.

D. TAC-CDFT calculations

The two-dimensional tilted axis cranking covariant density functional theory (TAC-CDFT) [22] is employed to study the observed bands in ^{195}Pt . In the calculations, the point-coupling covariant density functional PC-PK1 [23] is adopted and pairing correlations are neglected. The Dirac equation for the nucleons is solved in a 3D Cartesian harmonic oscillator basis with 12 major shells. More details about the calculations may be found in Ref. [24].

For the subsequent discussion, the following nomenclature will be used to denote bands in ^{195}Pt : Band 1 for the sequence feeding the $13/2^+$ band head, Band 2 for the negative-parity states up to $I^\pi = 33/2^-$, Band 3 for the rotation-aligned sequence built on the $33/2^+$ state, and Band 4 for the sequence built on the $(45/2^+)$ level. The self-consistent TAC-CDFT calculations have been performed based on the configurations $\pi(sd)^{-4} \otimes \nu(i_{13/2})^{-1}(fp)^4$ and $\pi(sd)^{-4} \otimes \nu(i_{13/2})^{-2}(fp)^5$ for Bands 1 and 2, respectively. In the vicinity of the $33/2^+$ level, Band 3 is assigned the configuration $\pi(sd)^{-4} \otimes \nu(i_{13/2})^{-3}(fp)^6$ which is realized from the alignment of a pair of neutrons from the $i_{13/2}$ subshell. A configuration change is evident around the $I^\pi = (45/2^+)$ state. The $\pi(h_{11/2})^{-2}(sd)^{-2} \otimes \nu(i_{13/2})^{-3}(fp)^6$ configuration, with the involvement of a pair of protons from the $h_{11/2}$ shell, is responsible for the high spin part of Band 3.

The calculated values of spin I versus rotational frequency $\hbar\omega$ and their comparison with experimental data are displayed in Fig. 11. The trends of the experimental data for Bands 2 and 3 are reproduced reasonably well, confirming the proposed configuration assignments. The tilted angles in the TAC-CDFT calculations are obtained self-consistently by minimizing the total Routhian for a given rotational frequency and configuration. For Bands 1, 2 and 3, the tilted angles are all $\theta=90^\circ$, indicating principal axis rotation along the long axis.

The calculated energy spectra and their comparison with data are found in Fig. 12. Since pairing correlations were not considered in the present calculations, the energy spectra are shifted by an appropriate amount (≈ 1 MeV) for comparison with experimental data. Additionally, $B(E2)$ values calculated for various configurations are also illustrated in Fig. 12. In general, these $B(E2)$ values are predicted to decrease with increasing spin. This reduction can be understood in terms of a decrease in collectivity and a transition from oblate to triaxial shapes described earlier in the context of UC calculations. A similar

trend is evident from TAC-CDFE calculations. $B(E2)$ values for the various configurations listed are quite different in magnitude and may be used to distinguish between different possibilities, once lifetime measurements become available from experiment.

IV. SUMMARY

The evolution of structure in odd- A Pt isotopes has been studied. High-spin levels with possible spin beyond $25 \hbar$ have been established in $^{193,195}\text{Pt}$. The existence of previously identified isomeric states in $^{193,197}\text{Pt}$ has been confirmed and a new one with $T_{1/2} = 5.0(5)$ ns was established in ^{195}Pt . Rotational bands in $^{193,195}\text{Pt}$ exhibit evidence for collectivity associated with moderate oblate deformation. Angular momentum at high spin in the positive-parity bands is generated by successive alignments of $i_{13/2}$ neutrons and $h_{11/2}$ protons. In ^{197}Pt , the previously observed isomer is confirmed and a few γ rays feeding this level have been identified. The rotational properties are explained in terms of cranking calculations using standard Nilsson parameters as well as others using tilted axis cranking covariant density functional theory.

V. ACKNOWLEDGMENTS

The authors would like to thank I. Ahmad, J.P. Greene, A.J. Knox, D. Peterson, U. Shirwadkar, X. Wang and C.M. Wilson for assistance during the experiment. SGW acknowledges support from the INSPIRE PhD Fellowship of the Department of Science and Technology, Government of India (Fellowship No. IF150098). SKT would like to acknowledge support from the University Grants Commission, India. This work is supported by the U.S. Department of Energy, Office of Science, Office of Nuclear Physics, under award numbers DE-FG02-94ER40848, DE-FG02-94ER40834, DE-FG02-97ER41033 and DE-FG02-97ER41041, and contract number DE-AC02-06CH11357. The research described here utilized resources of the ATLAS facility at ANL, which is a DOE Office of Science user facility.

-
- [1] R. R. Hilton and H. J. Mang, Phys. Rev. Lett. **43**, 1979 (1979).
 - [2] S.K. Tandel, EPJ Web of Conferences **107**, 03005 (2016).

- [3] S.G. Wahid, S.K. Tandel, P. Chowdhury, R.V.F. Janssens, M.P. Carpenter, T.L. Khoo, F.G. Kondev, T. Lauritsen, C.J. Lister, D. Seweryniak, and S. Zhu, *Phys. Rev. C* **92**, 054323 (2015).
- [4] X.H. Zhou *et al.*, *Phys. Rev. C* **75**, 034314 (2007).
- [5] T. Kutsarova, C. Schuck, E. Gueorguieva, A. Minkova, I. Zartova, F. Hannachi, A. Korichi, and A. Lopez-Martens, *Eur. Phys. J. A* **23**, 69 (2005).
- [6] Y.H. Zhang *et al.*, *Phys. Rev. C* **80**, 034303 (2009).
- [7] S.K. Saha, M. Piiparinen, J.C. Cunnane, P.J. Daly, C.L. Dors, T.L. Khoo, and F.M. Bernthal, *Phys. Rev. C* **15**, 94 (1977).
- [8] Y.D. Fang *et al.*, *Phys. Rev. C* **84**, 017301 (2011).
- [9] R. V. F. Janssens and F. S. Stephens, *Nucl. Phys. News* **6**, 9 (1996).
- [10] I-Yang Lee, *Nucl. Phys.* **A520**, c641 (1990).
- [11] S. J. Steer, Zs. Podolyak, S. Pietri, M. Gorska, H. Grawe, K. H. Maier, P. H. Regan, D. Rudolph, A. B. Garnsworthy, R. Hoischen *et al*, *Phys. Rev. C* **84**, 044313 (2011).
- [12] T. Kibedi, T.W. Burrows, M.B. Trzhaskovskaya, P.M. Davidson, C.W. Nestor, Jr., *Nucl. Instr. and Meth. A* **589**, 202 (2008).
- [13] H. Ton, G.H. Dulfer, J. Brasz, R. Kroondijk, J. Blok, *Nucl. Phys. A* **153**, 129 (1970).
- [14] S. A. Hjorth, A. Johnson, Th. Lindblad, L. Funke, P. Kemnitz, G. Winter, *Nucl. Phys.* **A262**, 328 (1976).
- [15] J. C. Cunnane, M. Piiparinen, P. J. Daly, C. L. Dors, T. L. Khoo, and F. M. Bernthal, *Phys. Rev. C* **13** , 2197 (1976).
- [16] R. Tischler, D. Mertin, A.H. El Farrash, B.V.T. Rao, R. Kroth, A. Kleinrahm, C. Gunther, H. Hubel, *Z. Phys. A* **288**, 67 (1978).
- [17] P. Schuler, J. Recht, H. Wilzek, K. Hardt, C. Gunther, K.P. Blume, K. Euler, V. Kolschbach, *Z. Phys. A* **317**, 313 (1984).
- [18] T. Bengtsson, *Nucl. Phys.* **A512**, 124 (1990).
- [19] S.K. Tandel, S.G. Wahid, P. Chowdhury, R.V.F. Janssens, M.P. Carpenter, T.L. Khoo, F.G. Kondev, T. Lauritsen, C.J. Lister, D. Seweryniak, S. Zhu, *Phys. Lett. B* **750**, 225 (2015).
- [20] S.K. Tandel, P. Chowdhury, E.H. Seabury, I. Ahmad, M.P. Carpenter, S.M. Fischer, R.V.F. Janssens, T.L. Khoo, T. Lauritsen, C.J. Lister, D. Seweryniak, Y.R. Shimizu, *Phys. Rev. C* **73**, 044306 (2006).

- [21] S. K. Tandel, A. J. Knox, C. Parnell-Lampen, U. S. Tandel, P. Chowdhury, M. P. Carpenter, R. V. F. Janssens, T. L. Khoo, T. Lauritsen, C. J. Lister, D. Seweryniak, X. Wang, S. Zhu, D. J. Hartley, Jing-ye Zhang, *Phys. Rev. C* **77**, 024313 (2008).
- [22] P. W. Zhao, S. Q. Zhang, J. Peng, H. Z. Liang, P. Ring, and J. Meng, *Phys. Lett. B* **699**, 181 (2011).
- [23] J. Meng, J. Peng, S. Q. Zhang, and P. W. Zhao, *Front. Phys.* **8**, 55 (2013).
- [24] J. Meng, *Relativistic Density Functional for Nuclear Structure* (World Scientific, Singapore, 2015).
- [25] R. Bengtsson, S. Frauendorf, F.-R. May, *At. Data and Nucl. Data Tables* **35**, 15 (1986).

TABLE I: Energies and intensities of γ rays, and excitation energies and spins of initial and final states in ^{193}Pt . DCO ratios are also presented, where available. Typical values of DCO ratios in gates on $E2$ transitions were found to be ≈ 1.0 and 0.5 for known stretched quadrupole and dipole γ rays, respectively. Transition energies are accurate to within 0.5 keV. Statistical uncertainties on γ -ray intensities and DCO ratios are listed.

E_γ (keV)	E_i (keV)	\rightarrow	E_f (keV)	I_i^π	\rightarrow	I_f^π	I_γ	DCO ratio
(122)	3595	\rightarrow	3473	—	\rightarrow	—		
133.9	1455	\rightarrow	1321	$25/2^{(-)}$	\rightarrow	$21/2^{(-)}$	25.7(15)*	
197.7	4732	\rightarrow	4534	—	\rightarrow	—	2.3(3)	
221.4	3816	\rightarrow	3595	—	\rightarrow	—	4.1(4)	
235.2	1690	\rightarrow	1455	$27/2^{(-)}$	\rightarrow	$25/2^{(-)}$	13.0(8)	
279.1	4201	\rightarrow	3922	$(49/2^+)$	\rightarrow	$(45/2^+)$	2.4(2)	
302.2	1992	\rightarrow	1690	$(29/2^-)$	\rightarrow	$27/2^{(-)}$	4.5(5)	
320.7	520	\rightarrow	199	$15/2^+$	\rightarrow	$11/2^+$	54.2(38)*	
327.2	2319	\rightarrow	1992	$(31/2^-)$	\rightarrow	$29/2^{(-)}$	2.4(3)	
340.1	1321	\rightarrow	981	$21/2^{(-)}$	\rightarrow	$19/2^+$	74.7(75)*	
341.2	491	\rightarrow	150	$17/2^+$	\rightarrow	$13/2^+$	100*	0.93(4)
343.7	3473	\rightarrow	3129	$41/2^+$	\rightarrow	$37/2^+$	5.2(4)	0.93(8)

E_γ (keV)	E_i (keV)	\rightarrow	E_f (keV)	I_i^{π}	\rightarrow	I_f^{π}	L_γ	DCO ratio
360.9	2696	\rightarrow	2335	$33/2^+$	\rightarrow	$29/2^+$	13.9(6)	0.90(5)
369.9	520	\rightarrow	150	$15/2^+$	\rightarrow	$13/2^+$	15.0(12)*	
432.8	3129	\rightarrow	2696	$37/2^+$	\rightarrow	$33/2^+$	12.6(6)	1.11(6)
448.4	3922	\rightarrow	3473	$(45/2^+)$	\rightarrow	$41/2^+$	2.9(3)	
460.9	981	\rightarrow	520	$19/2^+$	\rightarrow	$15/2^+$	50.1(35)*	
465.7	3595	\rightarrow	3129	—	\rightarrow	$37/2^+$	3.8(3)	
489.7	981	\rightarrow	491	$19/2^+$	\rightarrow	$17/2^+$	34.6(28)*	
504.1	3102	\rightarrow	2598	$(37/2^-)$	\rightarrow	$(33/2^-)$	6.1(6)	
512.4	1003	\rightarrow	491	$21/2^+$	\rightarrow	$17/2^+$	35.0(53)*	0.87(3)
537.2	1992	\rightarrow	1455	$29/2^{(-)}$	\rightarrow	$25/2^{(-)}$	14.2(17)*	
605.7	2598	\rightarrow	1992	$(33/2^-)$	\rightarrow	$29/2^{(-)}$	9.6(8)	
613.0	4814	\rightarrow	4201	$(53/2^+)$	\rightarrow	$(49/2^+)$	2.4(2)	
628.5	1632	\rightarrow	1003	$25/2^+$	\rightarrow	$21/2^+$	22.8(23)*	0.95(5)
629.2	2319	\rightarrow	1690	$(31/2^-)$	\rightarrow	$27/2^{(-)}$	5.2(6)	
672.0	4488	\rightarrow	3816	—	\rightarrow	—	2.3(3)	
(696)	(3770)	\rightarrow	3074	$(39/2^-)$	\rightarrow	$(35/2^-)$		

E_γ (keV)	E_i (keV)	\rightarrow	E_f (keV)	I_i^π	\rightarrow	I_f^π	L_γ	DCO ratio
703.4	2335	\rightarrow	1632	$29/2^+$	\rightarrow	$25/2^+$	19.5(9)	1.10(5)
718.1	4534	\rightarrow	3816	—	\rightarrow	—	2.0(3)	
755.1	3074	\rightarrow	2319	$(35/2^-)$	\rightarrow	$(31/2^-)$	4.4(6)	

Intensities of γ rays marked with an asterisk () are adapted from Ref. [7] since the presence of strong 340- and 341-keV transitions in coincidence with each other led to difficulties in extracting the values from the present data.

TABLE II: Energies and intensities of γ rays, and excitation energies and spins of initial and final states in ^{195}Pt . DCO ratios are also presented where available. Typical values of DCO ratios in gates on $E2$ transitions were found to be ≈ 1.0 and 0.5 for known stretched quadrupole and dipole γ rays, respectively. Transition energies are accurate to within 0.5 keV. Statistical uncertainties on γ -ray intensities and DCO ratios are listed.

E_γ (keV)	E_i (keV)	\rightarrow	E_f (keV)	I_i^π	\rightarrow	I_f^π	I_γ	DCO
144.1	1536	\rightarrow	1392	$25/2^-$	\rightarrow	$21/2^-$	35.5(19)	1.10(19)
174.2	2766	\rightarrow	2592	—	\rightarrow	$33/2^-$	3.6(3)	
181.4	1717	\rightarrow	1536	—	\rightarrow	$25/2^-$	10.6(7)	
185.5	1392	\rightarrow	1206	$21/2^-$	\rightarrow	$21/2^+$	25.4(33)	
204.5	1392	\rightarrow	1187	$21/2^-$	\rightarrow	$19/2^+$	84.3(43)	0.66(7)
225.9	3183	\rightarrow	2957	$37/2^+$	\rightarrow	$33/2^+$	8.2(5)	1.01(17)
246.0	4627	\rightarrow	4381	$(49/2^+)$	\rightarrow	$(45/2^+)$	1.7(1)	
304.6	2897	\rightarrow	2592	—	\rightarrow	$33/2^-$	4.2(4)	
314.6	3272	\rightarrow	2957	—	\rightarrow	$33/2^+$	2.9(3)	
364.8	2957	\rightarrow	2592	$33/2^+$	\rightarrow	$33/2^-$	22.3(9)	0.53(11)
368.5	628	\rightarrow	259	$17/2^+$	\rightarrow	$13/2^+$	100	0.81(8)
375.1	3272	\rightarrow	2897	—	\rightarrow	—	2.9(3)	

E_γ (keV)	E_i (keV)	\rightarrow	E_f (keV)	I_i^π	\rightarrow	I_f^π	L_γ	DCO
381.3	4670	\rightarrow	4289	—	\rightarrow	—	2.0(2)	
407.3	5034	\rightarrow	4627	(53/2 ⁺)	\rightarrow	(49/2 ⁺)	1.8(1)	
411.5	1947	\rightarrow	1536	29/2 ⁻	\rightarrow	25/2 ⁻	48.7(14)	1.07(8)
428.9	1187	\rightarrow	758	19/2 ⁺	\rightarrow	15/2 ⁺	20.0(15)	
447.5	3630	\rightarrow	3183	(41/2 ⁺)	\rightarrow	37/2 ⁺	6.5(5)	
499.3	758	\rightarrow	259	15/2 ⁺	\rightarrow	13/2 ⁺	28.5(18)	
559.6	1187	\rightarrow	628	19/2 ⁺	\rightarrow	17/2 ⁺	64.3(28)	
578.2	1206	\rightarrow	628	21/2 ⁺	\rightarrow	17/2 ⁺	35.7(22)	
645.0	2592	\rightarrow	1947	33/2 ⁻	\rightarrow	29/2 ⁻	29.2(12)	0.87(7)
662.2	4289	\rightarrow	3627	—	\rightarrow	—	3.4(3)	
675.1	5709	\rightarrow	5034	(57/2 ⁺)	\rightarrow	(53/2 ⁺)	1.5(1)	
709.2	1915	\rightarrow	1206	(25/2 ⁺)	\rightarrow	21/2 ⁺	6.8(4)	
750.4	4381	\rightarrow	3630	(45/2 ⁺)	\rightarrow	(41/2 ⁺)	2.8(3)	
773.4	2688	\rightarrow	1915	(29/2 ⁺)	\rightarrow	(25/2 ⁺)	3.4(3)	
860.2	3627	\rightarrow	2766	—	\rightarrow	—	4.0(4)	

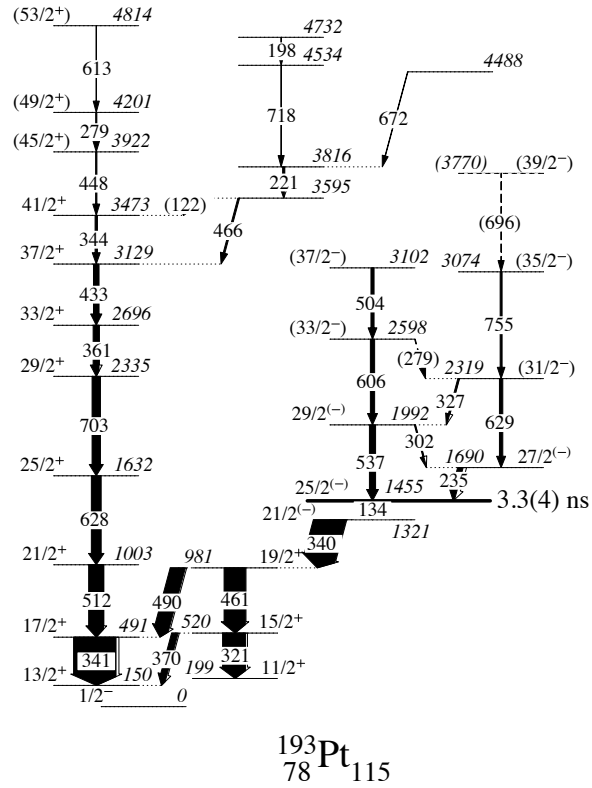


FIG. 1: Partial level scheme for ${}^{193}\text{Pt}$. Transitions above the $37/2^+$ state are new. Several new transitions are also observed in the negative-parity sequence.

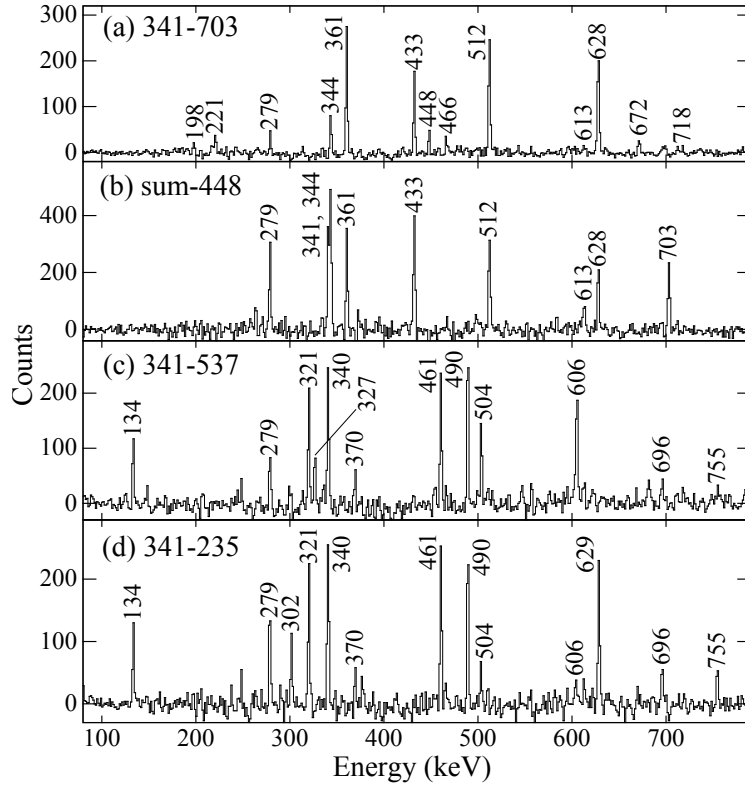


FIG. 2: Triple-gamma coincidence spectra displaying transitions assigned to the positive- and negative-parity sequences in ^{193}Pt . The gating transitions are indicated; details may be found in the text.

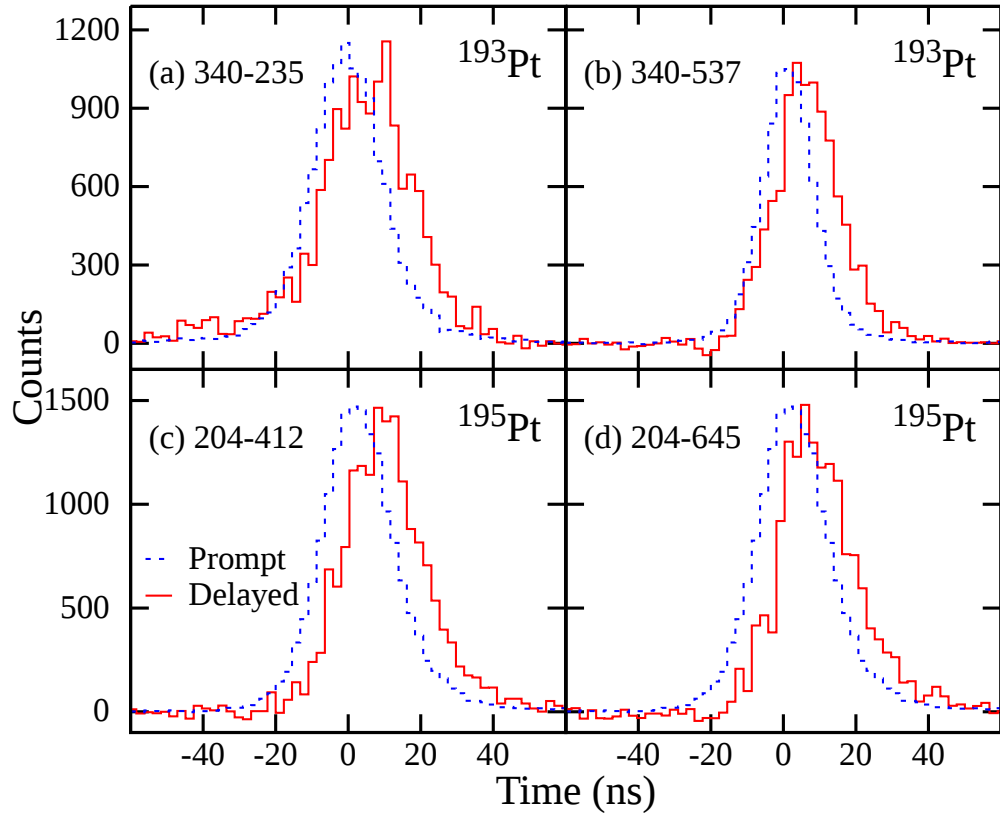


FIG. 3: (Color online) Half-life measurement using the centroid-shift technique: (a) and (b) $T_{1/2} = 3.3(4)$ ns for the $25/2^-$ state in ^{193}Pt ; (c) and (d) $T_{1/2} = 5.0(5)$ ns for the $25/2^-$ state in ^{195}Pt . The solid (red) curve displays the time difference between transitions deexciting and feeding the isomer, while the dotted (blue) one is that characteristic of prompt transitions with similar energies.

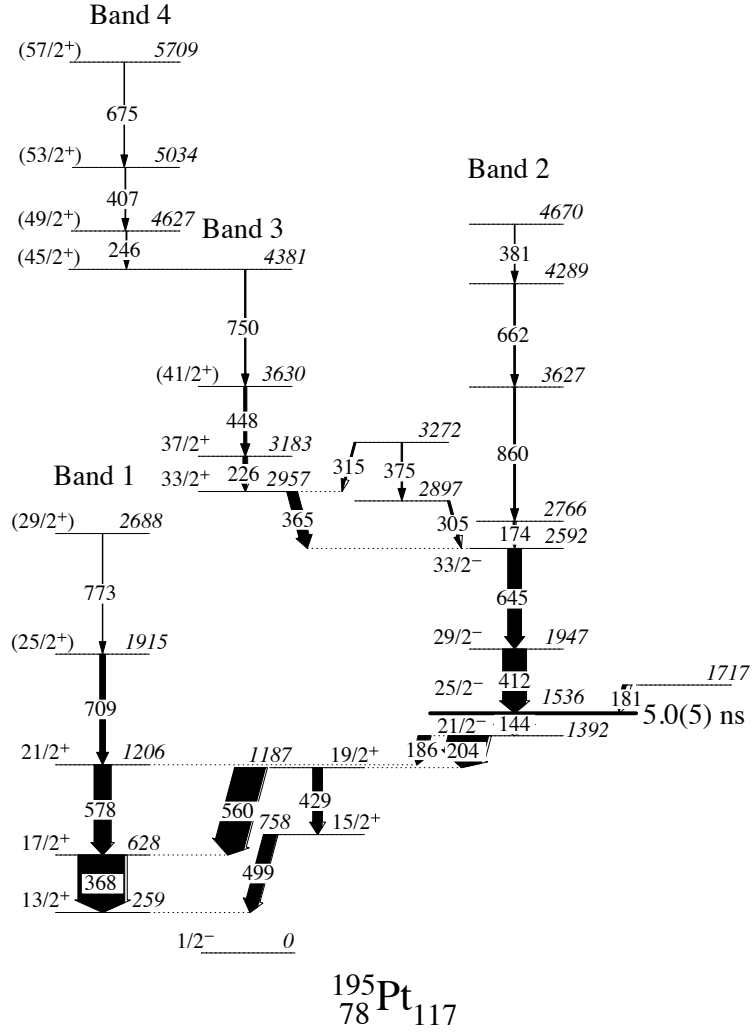


FIG. 4: Partial level scheme for ^{195}Pt illustrating transitions observed in the present work. All transitions above the $33/2^-$ level are new. The half-life of the $25/2^-$ level ($T_{1/2} = 5.0(5)$ ns) is newly determined.

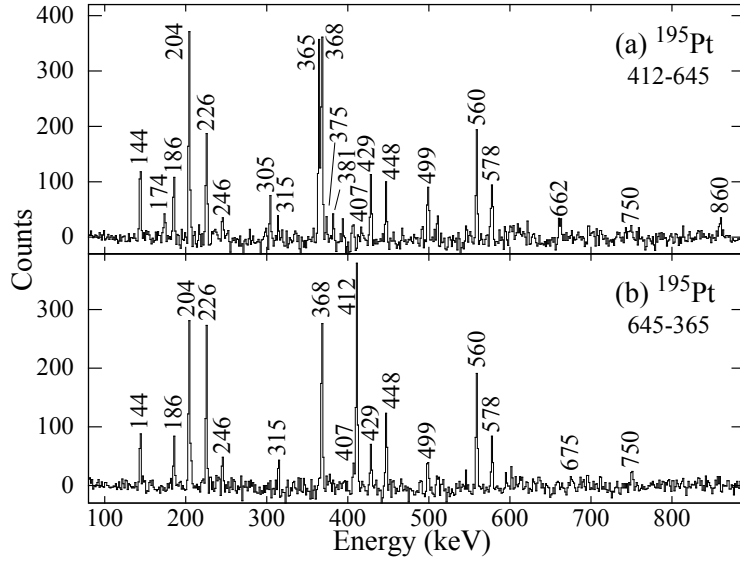


FIG. 5: Triple-gamma coincidence spectra displaying transitions in the positive- and negative-parity sequences in ^{195}Pt . The gating transitions are indicated.

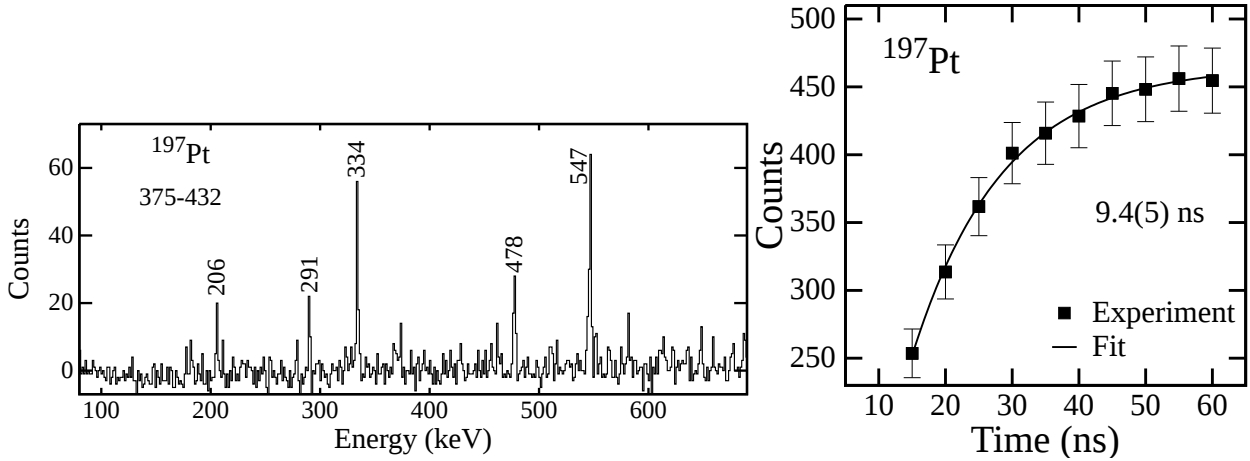
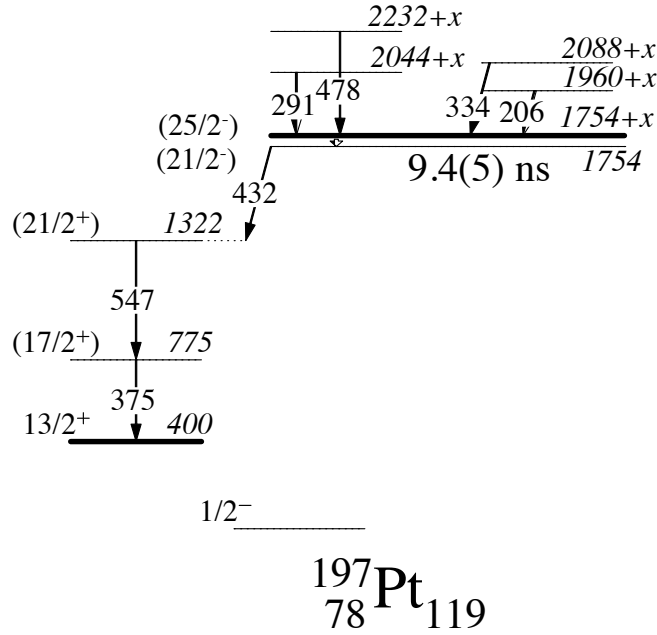


FIG. 6: Partial level scheme for ^{197}Pt illustrating transitions observed in the present work; those above the isomer are new. Triple-gamma coincidence spectrum displaying transitions in ^{197}Pt . Time variation of the integrated number of coincidence counts in delayed transitions (375 and 432 keV) from the decay of the $I^\pi=25/2^-$ level in ^{197}Pt indicating $T_{1/2}=9.4(5)$ ns.

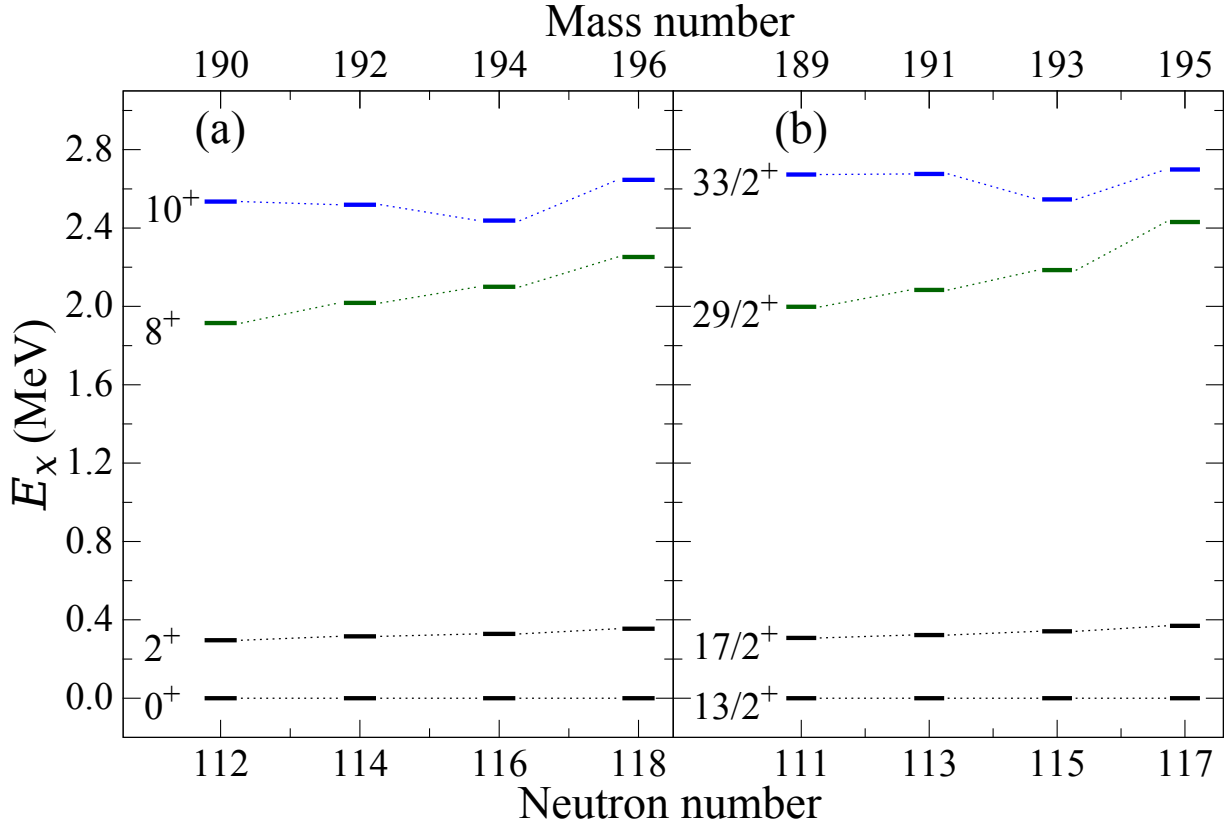


FIG. 7: (Color online) Systematic comparison of the excited level structure in even- and odd- A Pt isotopes from $^{189-196}\text{Pt}$. Note that the excitation energy of the $13/2^+$ state in the odd- A isotopes is offset by an amount equal to its excitation energy (typically a few hundred keV) to facilitate the comparison. A detailed discussion is presented in the text.

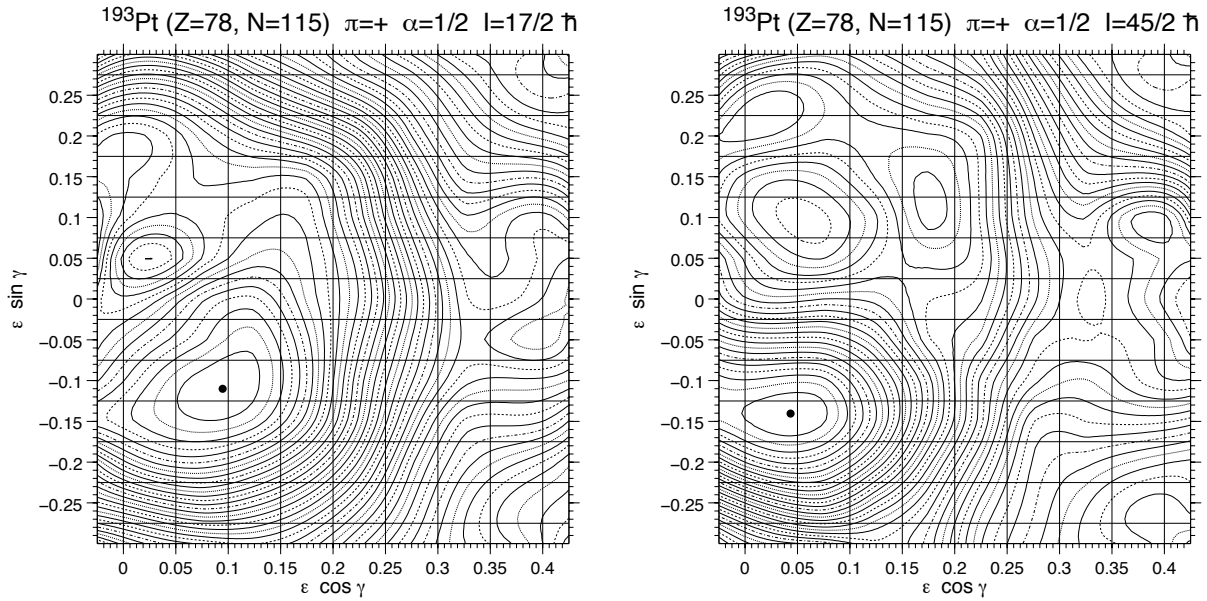


FIG. 8: Total Energy Surface plots illustrating energy minima in the positive-parity, yrast structure in ^{193}Pt for different values of spin from calculations performed using the Ultimate Cranker code [18]. It is evident that the lowest energy minimum is nearly oblate ($\epsilon_2=0.145$, $\gamma \approx -50^\circ$) at low spin: $I=17/2 \hbar$ with a gradual transition towards a triaxial shape ($\gamma = -74^\circ$ at $I=45/2 \hbar$) at higher spin. The spacing between adjacent energy contours is 200 keV.

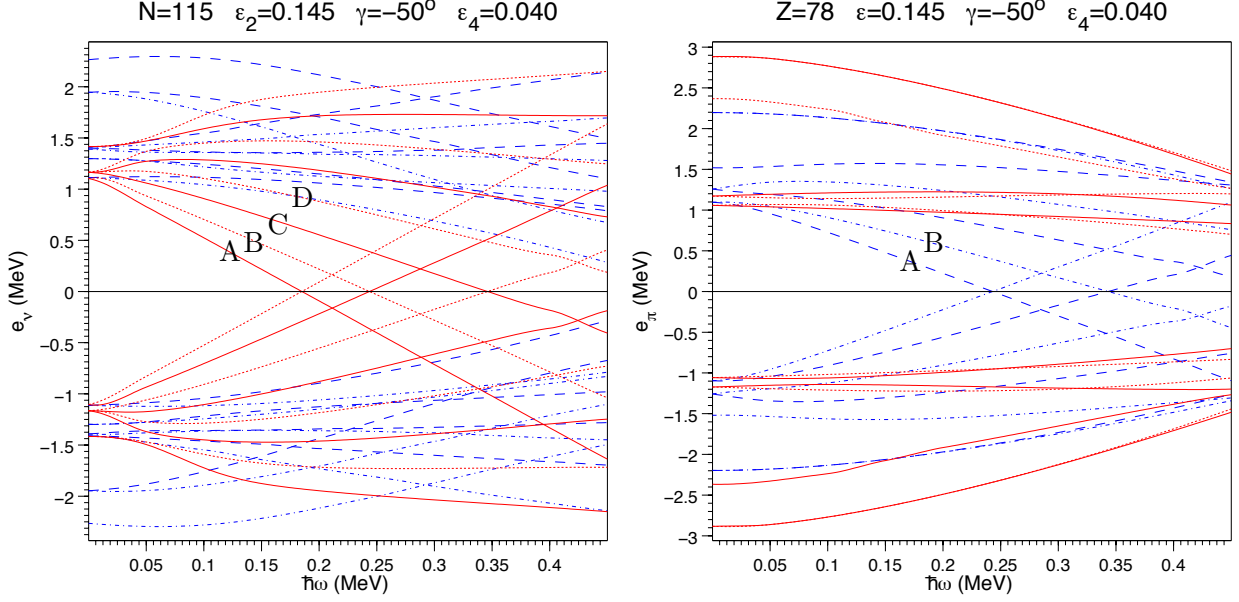


FIG. 9: (Color online) Neutron and proton quasiparticle energies in ^{193}Pt calculated as a function of rotational frequency using the Ultimate Cranker code with standard Nilsson parameters. The letter labels A, B etc. follow the standard convention in the cranking model as listed in *e.g.* Ref. [25].

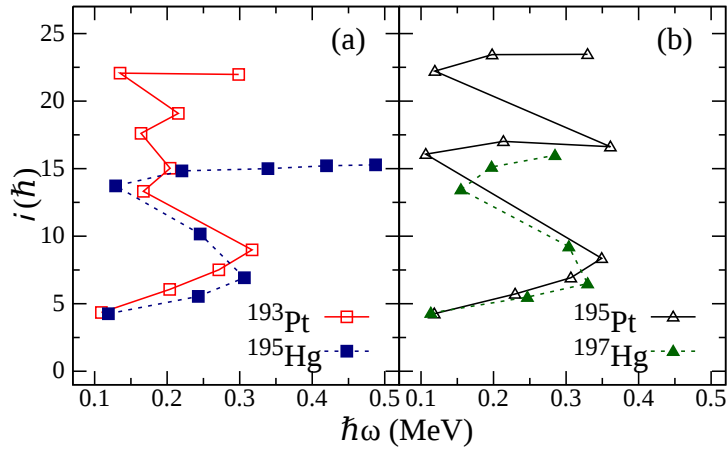


FIG. 10: (Color online) Aligned angular momentum as a function of rotational frequency for $^{193,195}\text{Pt}$ and $^{195,197}\text{Hg}$. A reference rotor with $J_0=8 \text{ } \hbar^2\text{MeV}^{-1}$ and $J_1=35 \text{ } \hbar^4\text{MeV}^{-3}$, appropriate for a comparison in this region, is used.

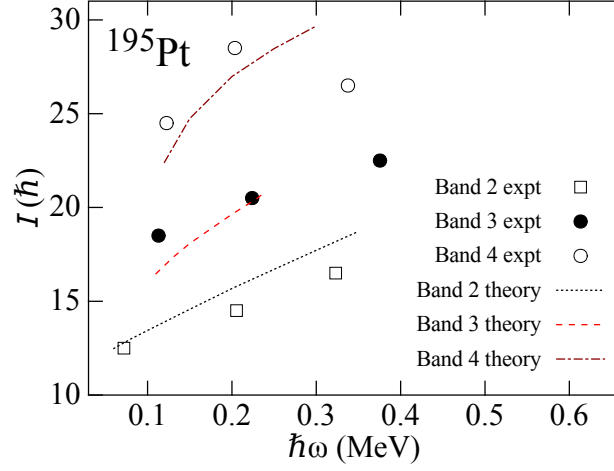


FIG. 11: (Color online) Spin as a function of rotational frequency for bands in ^{195}Pt from experiment and TAC-CDFT calculations.

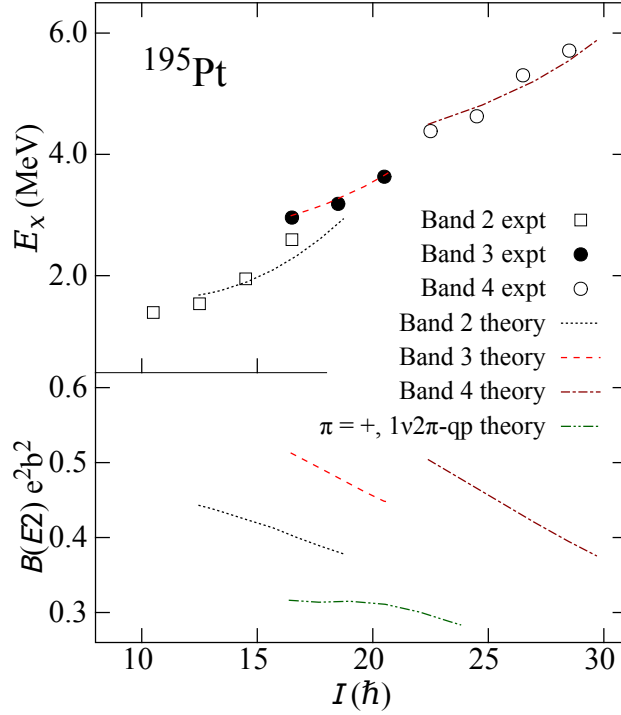


FIG. 12: (Color online) Evolution with spin of excitation energies and reduced $E2$ transition probabilities in ^{195}Pt from experiment and TAC-CDFT calculations. A detailed discussion is presented in the text.